Plasma Physics and Controlled Fusion, Vol. 32, No. 11, pp. 889 to 902, 1990.
Printed in Great Britain.

0741-3335/90 $3.00 + .00
IOP Publishing Ltd. and Pergamon Press plc.

HIGH POWER ICRH AND NB HEATING RESULTS IN TEXTOR

A.M. MESSIAEN[1*], H. CONRADS[2], M. GAIGNEAUX[1], J. ONGENA[1], R.R. WEYNANTS[1*], G. BERTSCHINGER[2], J.M. BEUKEN[1], P. CORNELISSEN[1], T. DELVIGNE[1], F. DURODIE[1], H.G. ESSER[2], H. EURINGER[2], G. FUCHS[2], B. GIESEN[2], B. GÖRG[2], D.L. HILLIS[3], F. HOENEN[2], P. HÜTTEMAN[2], M. JADOUL[1], R. KOCH[1], H. KEVER[2], M. KORTEN[2], W. KOHLHAAS[2], D. LEBEAU[1], M. LOCHTER[2], D. REITER[2], D. RUSBÜLDT[2], M. SAUER[2], J. SCHLUETER[2], H. SOLTWISCH[2], M. STORCH[2], G. TELESCA[1], R. UHLEMANN[2], P.E. VANDENPLAS[1], R. VAN NIEUWENHOVE[1], G. VAN OOST[1], G. VAN WASSENHOVE[1], G. WAIDMANN[2], J.G. WANG[4], J. WINTER[2], G.H. WOLF[2], J.W. YANG[4]

(1) Laboratoire de Physique des Plasmas - Laboratorium voor Plasmafysica
Association "Euratom-Etat belge" - Associatie "Euratom-Belgische Staat"
Ecole Royale Militaire - B-1040 Brussels - Koninklijke Militaire School

(2) Institut für Plasmaphysik, Forschungszentrum Jülich, GmbH
Association "Euratom-KFA", D-5170 Jülich, FRG

(3) Oak Ridge National Laboratory, P.O. Box X, Oak Ridge, TN 37831, USA

(4) Southwestern Institute of Physics, Leshan, Sichuan, PRC

(*) Researcher at NFSR, Belgium

ABSTRACT

Neutral beam injection (NBI-co and NBI-counter), ICRH and their combinations have been compared on TEXTOR for what concerns the heating and their effect on the energy anisotropy and the confinement. In most of the cases, stationary heated plasma conditions have been obtained with boronized wall. The main results are :
(i) Production of a hot ion mode with NBI-co. It is characterized by a large energy anisotropy, by a large non inductively driven toroidal current and by the stabilization of the sawteeth (of the monster type) due to the hot ion tail.
(ii) Significative enhancement of these effects when ICRH is added to NBI-co. The neutron yield is also increased by the addition of ICRH. Peak electron and ion temperature around 3 keV have been obtained and 70 % of the total current has been non inductively driven.
(iii) Large excess of the total energy content (up to 2.3) with respect to the L-mode scaling predictions has been obtained with the combinations NBI-co + ICRH or NBI-co + NBI-counter.
(iv) Up to 6 MW of additional power has been coupled to the plasma leading to β_p = 1.5 and β_t equal to 70 % of the Troyon limit.

KEYWORDS

Co-and counter-neutral beam injection - ICRH - combined heating - confinement - sawtooth stabilization - monster sawteeth - non inductively driven current.

1. INTRODUCTION

Auxiliary heating of TEXTOR has been carried out by means of co- and counter-beam injection and of ICRH. These heating methods and their combinations have been carefully compared.

During the reported experiments TEXTOR has been operated in the following conditions : plasma current I_p = 340 kA (except otherwise stated), toroidal field B_t = 2.25 T, small and large

plasma radii repectively of a = 46 cm and R = 175 cm with a plasma circular in shape and limited by the toroidal belt limiter ALT-II. The neutral beam system consists of one co - and one counter-beam line (Euringer et al., 1989), each equipped with one modified ion source of the type "JET-PINI", and for the present experiments, is injecting deuterium into a deuterium plasma, tangentially to the major radius R, with a beam voltage of 50-55 kV, a total power up to 2 x 1.7 MW and a beam divergence less than 1 degree. The beam power is split between the components at full, half and third energy respectively in the ratio ~ 69, 24 and 7 %. The ICRH set up consists of two independent heating lines (Messiaen et al., 1989a) each fed by one 2 MW generator operated at 32.5 MHz and connected to a pair of $\lambda/7$ antennae. Each pair of antennae is fed in phase opposition and provides a low field side RF excitation. Pure ICRH minority heating is used as heating scenario in a D-(H) plasma with a hydrogen concentration lower than 10 %. Second harmonic interaction with the ions of the beam cannot be excluded in the case of combined NBI - ICRH.

The present experiments are performed with boronized wall conditioning (described by Winter et al., 1989). Such a wall coating process allows operation with negligible contribution of the metallic impurities to the total radiation in presence of additional heating. It allows also stationary low impurity conditions and the minimization or avoidance of the density increase during the heating pulse. With ICRH, the use of antenna pairs fed in phase opposition further decreases the interaction with the wall and does not lead to a drop in plasma loading with respect to the in-phase feeding (Messiaen et al., 1989a, Weynants et al., 1989a). This has allowed us to couple in stationary conditions up to 90 % of the nominal power of the RF generators (i.e. 3.6 MW) with radiation losses remaining below 600 kW and a density controlled by feedback. The boronized wall condition also enables to obtain a stationary hot ion mode with co-injection (NBI-co) at low density. With combined NBI + ICRH heating an additional power up to 6 MW has been presently coupled to the plasma and the total plasma energy content (including the contribution of the tails) has reached 145 kJ at I_p = 340 kA and 180 kJ at I_p = 470 kA leading to a maximum value of $\beta_p = 1.5$ at 340 kA and 1.6 at 220 kA.

The main characteristics of each heating method and of their combinations will be discussed in the next sections. A first account on the NBI performances has been presented (Conrads et al., 1989). Detailed analysis of the ICRH results with the present low field side excitation has been reported (Messiaen et al., 1989a and Weynants et al. 1989a,b), and the first results of the combined operation NBI + ICRH are summarized in Messiaen et al., 1989b.

2. NBI - CO HEATING

From one operation day to another, NBI-co leads to a large scatter in the plasma energy content, for apparently the same machine conditions. Lower points have in about equal proportion a lower ion and electron energy content as well as a lower tail contribution. It is not yet clear how to reach the best energy conditions but it appears to be a prerequisite to have low recycling conditions and optimal positioning of the plasma. On Fig. 1 the extent of the scatter of the diamagnetic energy is shown. In the following, we will concentrate our analysis on results pertaining to a set of data of the best regime obtained in successive discharges.

NBI-co heating leads to strong non-thermal components when the central line averaged density $\bar{n}_{eo}$ is decreased. A typical shot description is given in Fig. 2 where the time evolution of the diamagnetic energy E_{dia}, the equilibrium (or MHD) energy E_{equi}, the central electron temperature T_{eo} (from ECE), the ion temperature $T_{i,19.5}$ (measured 19.5 cm off axis, i.e. at R = 1.945 m, by charge exchange spectroscopy), the loop voltage V_ℓ, the density $\bar{n}_{eo}$ (from HCN interferometer) and the total radiated power P_{rad} (from bolometry) are shown during a NBI pulse. The apparent stationarity of the plasma parameters, the large energy anisotropy, large central ion and electron temperatures, large loop voltage drop, and long sawtooth period are peculiar to the co-injection in TEXTOR. What is also apparent is the low ratio of P_{rad} to the total injected power P_{tot} (~0.25).

(i) Energy and temperature. The behaviour of E_{dia} and E_{equi} versus the density is shown in Fig. 3a. The electron contribution to the thermal component of the energy, E_{kin}, is computed from the HCN interferometer density profile $n_e(r)$ and the temperature profile $T_e(r)$ obtained from 9 ECE channels. The central temperature of ohmic plasmas is obtained from the neutron yield (assuming a Maxwellian distribution of the ions and an ion temperature profile homothetic to the electron one; the effect of Z_{eff} is also taken into account). The ionic energy component in auxiliary heated plasmas is

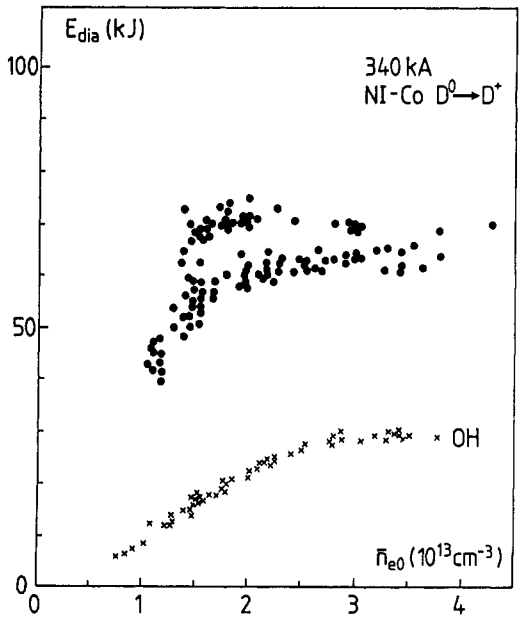

Fig. 1 E_{dia} versus $\bar{n}_{eo}$ for NBI-co heated shots (data of many operational days).
The OH values are also indicated.

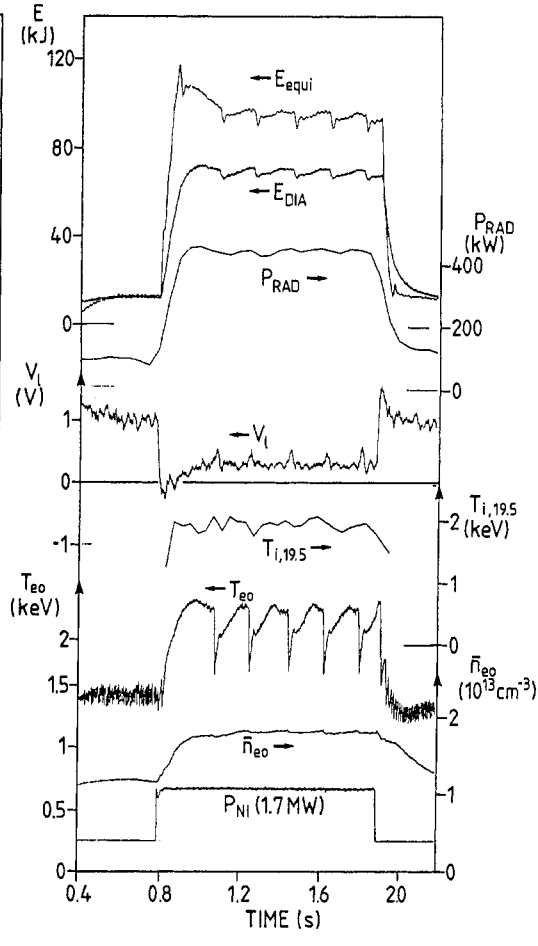

Fig. 2 Time evolution of E_{equi}, E_{dia}, P_{rad}, V_ℓ, $T_{i,19.5}$, T_{eo}, n_{eo}, P_{NI} during a NBI-co heated shot (# 37767).

rather poorly known, as the ion temperature is only measured with CXES in the presence of the co-beam and at one radial location. The actual magnetic surface on which this temperature prevails is found from the measured position of the magnetic axis. The ion temperature profile $T_i(r)$, and thus also the central value T_{io}, is computed by the code TRANSP of Princeton (Hawryluk et al., 1980) assuming neoclassical ion thermal diffusivity with a, radially constant, enhancement factor whose value is obtained by imposing the computed $T_i(r)$ to pass through the measured point. The ion contribution to E_{kin} is then computed by TRANSP correcting the ion density for impurities and beam particles. The agreement between the three energy values for ohmic discharges and for heated ones, at sufficiently large plasma density, is usually better then 10 %. Large differences develop however because of strong non-thermal components in NBI heated discharges at low density, as shown in Fig. 3a. The distribution of the tail energy among its parallel and perpendicular components $E_{//a}$ and $E_{\perp a}$ can be obtained from E_{dia}, E_{equi} and E_{kin}. The values thus obtained are confirmed by the predictions of TRANSP. On the other hand, note that the E_{kin} values can roughly be retrieved from the corresponding E_{equi} and E_{dia} values assuming the relation $E_{//a} \cong 2\, E_{\perp a}$, predicted by the TRANSP simulations. In Fig. 3a we also show : (i) the total energy content $E_{tot} = E_{kin} + E_{//a} + E_{\perp a} = (2\, E_{equi} + E_{dia})/3$ which includes the tail contribution and the thermal component of the energy E_{kin} and (ii) the prediction of the original scaling of Kaye and Goldston, 1985, which is noted K-G. For the computation of the total power P_{tot}, we have used the sum of the engineering value of the injected NBI power P_{NI}, without taking into account the charge exchange losses, and the remaining ohmic power $P_{OH} = V_\ell\, I_p$. At low density, E_{kin} is on the K-G scaling but the total energy E_{tot} is a factor 2.4

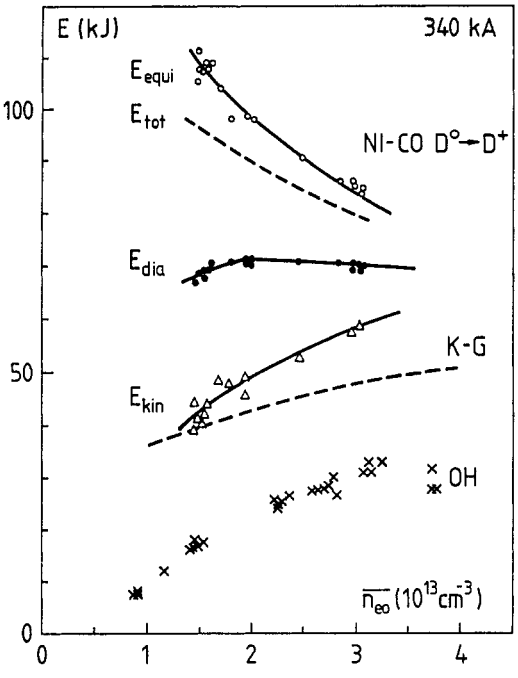

Fig. 3a Density scan of E_{equi}, E_{tot}, E_{dia} and E_{kin} during NBI-co. The corresponding predictions of the Kaye-Goldston scaling (noted K-G) and the OH values are also indicated.

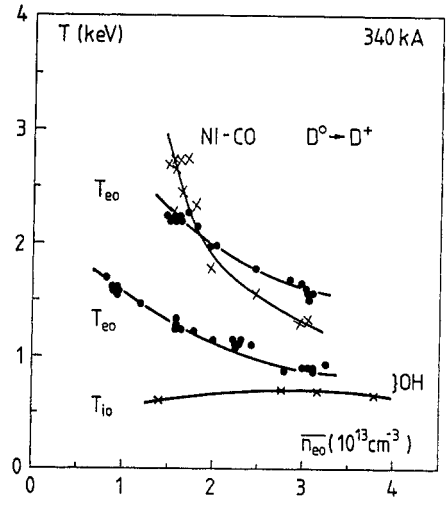

Fig. 3b T_{io} and T_{eo} values corresponding to Fig. 3a.

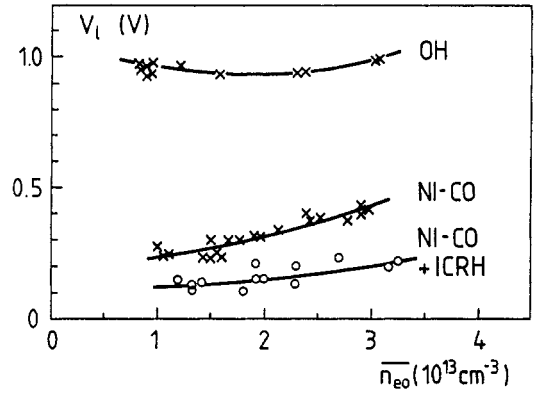

Fig. 3c V_ℓ evolution corresponding to Fig. 3a. The values obtained for combined heating NBI-co + ICRH ($1.5 < P_{RF} < 1.7$ MW) are also given.

above it, with an energy in the tails (E_{tot} - E_{kin}) which is larger than the thermal component E_{kin}. The fact that E_{dia} is above the Kaye-Goldston scaling is due to the existence of a perpendicular tail. In Fig. 3b are shown the central ion temperature T_{io} computed as explained above, together with T_{eo}; at a density $\overline{n}_{eo} = 1.5 \times 10^{13}$ cm^{-3}, T_{eo} is above 2 keV and T_{io} reaches 2.6 keV. The ohmic values of T_{eo} and T_{io} are also given for completeness in Fig. 3b.

(ii) Loop voltage. The loop voltage evolution versus density in ohmic condition and with NBI-co heating is shown in Fig. 3c. The large loop voltage drop due to NBI heating can only be partially explained by the decrease of resistivity. An evaluation of the total non-ohmically driven

current I_{tD} (due to beam driven and bootstrap current) is obtained by

$$I_{tD} = I_p - \frac{V_\ell}{2\pi R} \int \sigma_{NC} dA \qquad (1)$$

where σ_{NC} is the neoclassical resistivity and A the plasma cross section. The current I_{tD} varies from 180 kA to 110 kA when $\bar{n}_{eo}$ increases from 1.4 to 3 x 10^{13} cm^{-3}. At low density, more than half of the plasma current is non-ohmically driven. Simulations by TRANSP of these shots have been done with as input : the NBI characteristics, the profiles $N_e(r)$, $T_e(r)$ and the Z_{eff} value, the ion temperature profile obtained as explained in the preceeding paragraph. These simulations predict the values of V_ℓ, resulting from the plasma resistivity and the non-ohmically driven current, which are in good agreement with the experimental ones and show that the contribution of the bootstrap current to I_{tD} lies between 35 and 40 kA.

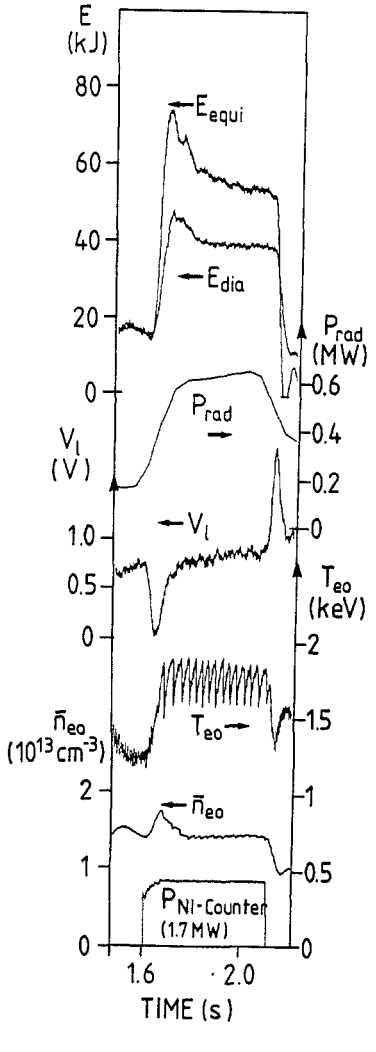

Fig. 4 Same data as in Fig. 2 but for a NBI-counter heated shot (# 41096).

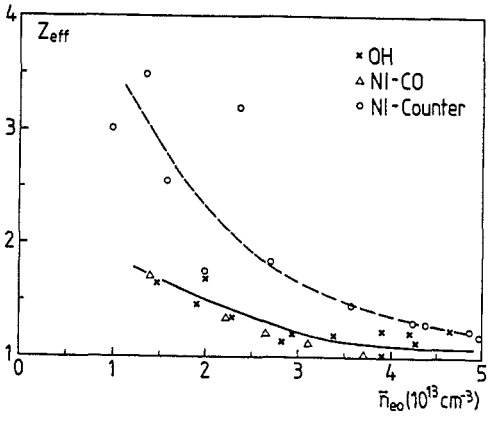

Fig. 5 Z_{eff} evolution versus $\bar{n}_{eo}$ for OH, NBI-co and NBI-counter conditions as measured by soft X rays.

(iii) Sawtooth stabilization. NBI-co heating is very efficient in stretching the sawtooth period as seen in Fig. 2. For a given value of P_{NI} the period increases monotonically when the density decreases and below a threshold density (~ 1.5 x 10^{13} cm^{-3} for the neutral beam conditions of Fig. 2) the sawteeth are completely stabilized, T_e remaining at its maximum value. A detailed analysis (Ongena et al., 1990) shows that the stabilized sawtooth is of the "monster" type with a central q below 1 and that the results can be interpreted in terms of stabilization of the resistive internal m = 1 mode by trapped energetic ions. The creation of trapped hot ion populations strongly peaked inside the q = 1 surface appears to be essential for the stabilization. Note that sawtooth stabilization with NBI has also been observed on ASDEX in divertor discharges (Söldner et al., 1986).

3. NBI-COUNTER HEATING AND COMPARISON WITH CO-INJECTION

A typical example of the time evolution of the plasma parameters during a NBI-counter pulse is given in Fig. 4 for a density comparable to that of the NBI-co shot of Fig. 2. It can be immediately appreciated that : (i) the difference between E_{dia} and E_{equi} is much smaller than for NBI-co and that the electron heating is also lower; (ii) the stationary loop voltage remains high; (iii) the sawtooth stretching is much smaller than for NBI-co.
The scatter of the energy measurements between the different days of operation is lower for counter-injection than for co-injection. The density increase produced by the NBI pulse is generally larger and higher values of Z_{eff} are obtained. This is shown in Fig. 5 where the measurement of Z_{eff} from soft X ray analysis for ohmic, co and counter discharges is displayed versus the density. When comparing the density scans of the energy shown on Fig. 3a and Fig. 6a, it appears that all the energies, including the tail energies, are lower for counter-injection. As there is no T_i measurement presently available in case of counter-injection, the value of E_{kin} is computed from E_{dia} and E_{equi} assuming the relation $E_{//a} = 2\,E_{\perp a}$ which is also verified for the NBI-counter shot simulations by

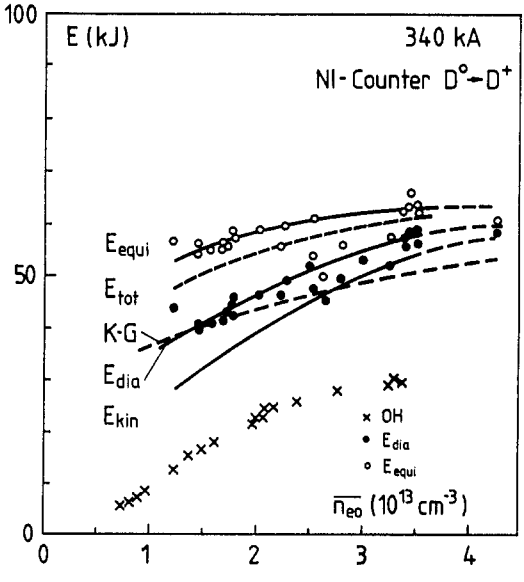

Fig. 6a Similar density scan as in Fig. 3a but for NBI-counter.

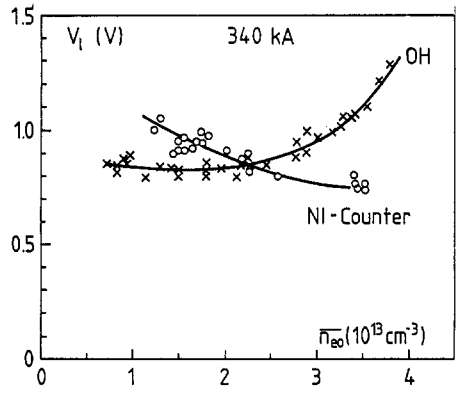

Fig. 6b V_ℓ versus $\bar{n}_{eo}$ corresponding to the conditions of Fig. 6a.

TRANSP. At $\bar{n}_{eo}$ = 2 x 10^{13} cm^{-3}, E_{tot} is only 62 % and E_{kin} 78 % of the corresponding value for the best co-injection conditions. At low density E_{kin} is lower than the K-G scaling. The lower heating efficiency is also confirmed by the lower increase of the central electron temperature observed with NBI-counter heating as shown in Fig. 12. At sufficiently large density the heating performance of NBI-counter is approaching that of NBI-co.
The loop voltage behaviour is shown in Fig. 6b. At low density the loop voltage can be even higher than the ohmic value during the NBI-counter pulse. Now the beam driven current is opposed to the ohmic one thus cancelling the loop voltage drop due to the electron heating and an enhanced bootstrap current.

A part of this increase of V_ℓ is also due to the rise of Z_{eff} shown in Fig. 5. TRANSP simulation of the shot shown in Fig. 4 leads to a value of I_{tD} = -60 kA from which -87 kA are due to beam driven current and 27 kA to bootstrap current.
It is shown that the much lower capability of counter-injection as compared to co-injection in stretching the sawtooth period can be understood by the differences in magnitude and in spatial distribution of the trapped hot ion population inside the q = 1 surface (Ongena et al., 1990). It appears also that, opposite to the NBI-co case, the sawtooth period observed with NBI-counter is roughly density independent and that no complete sawtooth stabilization is observed.

4. ICRF HEATING AND COMPARISON WITH NBI

The ICRH heating results pertaining to the minority heating in a (H)-D plasma with the present antenna system have been described and compared to theory (Beuken et al. ,1988 and Weynants et al., 1989a and b). The results of a power scan at fixed density $n_{eo} = 3 \times 10^{13}$ cm^{-3}, corresponding to the best performances achieved up to now on TEXTOR, are given in Fig. 7a for the energies, in Fig. 7b for the central temperatures and in Fig. 7c for the loop voltage. T_{eo} is obtained from ECE and T_{io} from the neutron yield. The values of T_{eo} are the same for NBI-co and ICRH and are lower for NBI-counter. The saturation appearing on the T_{eo} and T_{io} values with ICRH at high P_{tot} is correlated with density profile broadening. The energies and central electron temperatures corresponding to the best performances of NBI-co and NBI-counter are also shown for comparison in Fig. 7a and b. The difference $E_{dia} - E_{equi} = 3/4\ (E_{\perp a} - 2E_{//a})$, where $E_{\perp a}$ and $E_{//a}$ are respectively the energies of the perpendicular and parallel tails, is a measure of the tail anisotropy. For ICRH, the tail is almost completely perpendicular and $E_{dia} > E_{equi}$; for NBI-co and NBI-counter we have, as stated before, $E_{//}/E_{\perp} \cong 2$ and consequently $E_{equi} > E_{dia}$. In table 1 we give, for the same n_{eo} and I_p as for Fig. 7, the values of the incremental confinement times $\tau_{inc,tot}$ and $\tau_{inc,kin}$ corresponding respectively to E_{tot} and E_{kin}. We quote also the electron and ion heating efficiencies $\eta_\alpha = n_{eo}\,\Delta T_\alpha/P_{aux}$; where α stands for electrons or ions. As for the NBI power P_{NI}, we use for the ICRH power P_{RF} the engineering value of the power, i.e. the power radiated into the tokamak, to compute P_{tot} and $P_{aux} = P_{NI} + P_{RF}$.

Table 1 : τ_{inc} and η_α corresponding to Fig. 7

	unit	NBI-co	NBI-counter	ICRH
$\tau_{inc,tot}$	ms	32	18	17
$\tau_{inc,kin}$	ms	18	12	12
$n_{eo}\Delta T_e/P_{aux}$	keV 10^{13} cm^{-3}/MW	1.25	0.78	0.95
$n_{eo}\Delta T_i/P_{aux}$	"	1.46		0.77

From Fig. 7a and Table 1 it appears that the confinement times for the total energy or its thermal part are larger for the best NBI-co conditions and are the same for the best NBI-counter and ICRH results. The ion contribution to the thermal energy E_{kin} is the largest for NBI-co and the smallest for ICRH.
On Fig. 7c we have compared the measured loop voltage values with those computed from neoclassical resistivity including bootstrap current. A good agreement is observed. The influence of ICRH on the sawteeth period has been discussed in Weynants et al., 1989b.

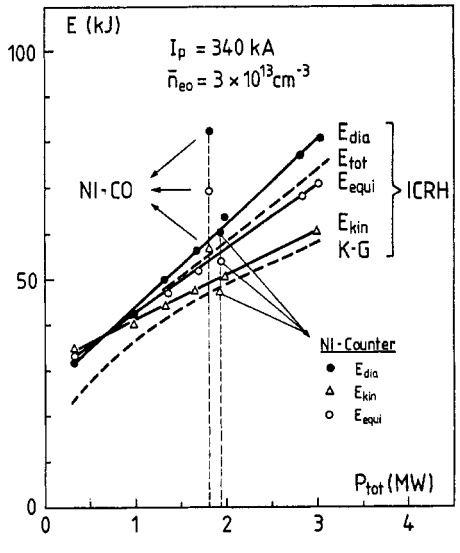

Fig. 7a Power scan of E_{equi}, E_{tot}, E_{dia}, E_{kin} for ICRH. The representative points for NBI-co and NBI-counter heating conditions are given for comparison. The corresponding K-G scaling is also shown.

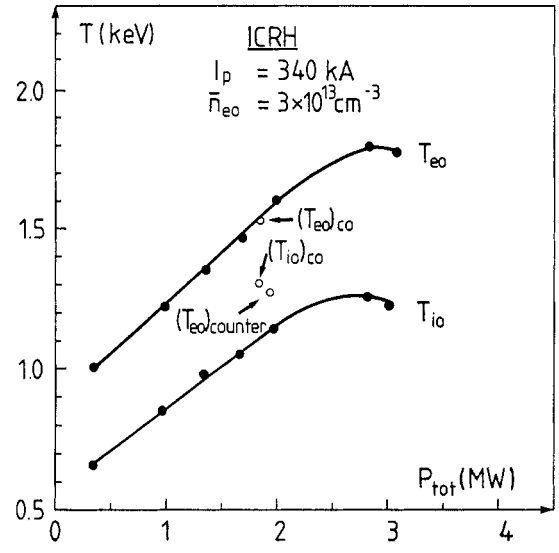

Fig. 7b T_{eo} and T_{io} evolution corresponding to Fig. 7a.

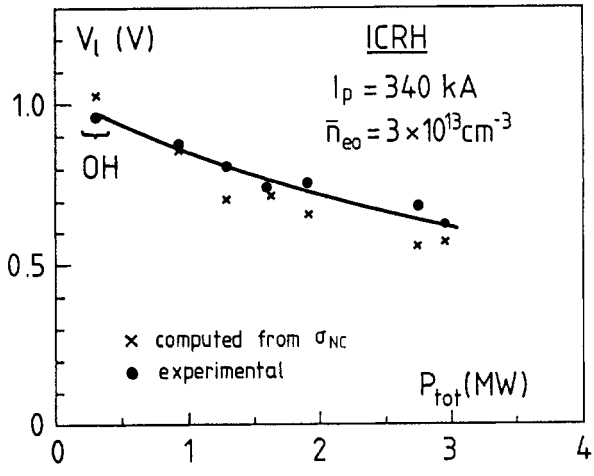

Fig. 7c

Power scan of V_ℓ with ICRH. The crosses indicate the results of V_ℓ computation (using σ_{NC} and taking into account I_{BS}).

5. COMBINED HEATING SCHEMES

5.1 Combined NBI-co and ICRH.

Figure 8 illustrates the evolution of plasma parameters during a NBI-co pulse to which an ICRH pulse of the same power is added. The effects induced by the addition of ICRH are striking :

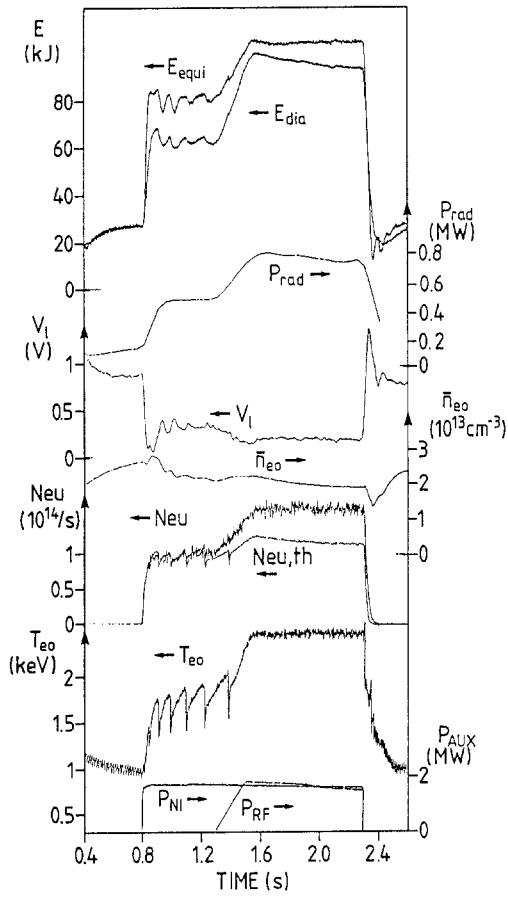

Fig. 8 Time evolution of E_{equi}, E_{dia}, P_{rad}, V_ℓ, $\bar{n}_{eo}$, the neutron yield Neu, T_{eo}, P_{NI}, P_{RF} during a NI-co followed by NBI-co + ICRH heated shot (# 41130).
Neu,th gives the prediction of a theoretical model.

(i) It produces a more "isotropic" tail, i.e. $E_\perp \cong 2E_{//}$, as seen from the evolution of the energies. A detailed analysis shows that $E_{//}$ remains unchanged within the error bar and that the effect of ICRH is to increase $E_\perp$ roughly from $E_{//}/2$ to $2E_{//}$. The effect on the total energy and on its thermal part is shown in Fig. 9a. The doubling of the tail energy content results from the formation by ICRH of its own minority energetic tail and from the enhancement of the energy slowing down time of the beam due to the hotter target plasma. The possibility of a further direct interaction between RF and beam particles will be discussed in Conrads et al., 1990. The increase of the central electron temperature and of the ion temperature measured by charge exchange emission 19.5 cm off axis (i.e. at r/a = 0.25 to 0.30 depending on the exact position of the magnetic axis) are shown in Fig. 9b and 9c. Large outward shifts of the electron and density profiles are observed caused by the high value of β_p. A peaking of both profiles with respect to the OH condition also occurs.

(ii) A further reduction of the loop voltage, which remains stationary during combined heating, is observed. The corresponding experimental points are shown in Fig. 3c. Such an additional drop is a result of a complex balance between the decreased resistivity and the increased beam slowing down due to the hotter target plasma, and a possible direct interaction of the RF and the beam at $\omega = 2\,\omega_{CD}$ resulting in increased slowing down as well as possible increased particle trapping. The increase of the total non inductively driven current I_{tD} can be obtained from Equ. (1). At $\bar{n}_{eo} = 1.7 \times 10^{13} cm^{-3}$, I_{tD} rises from 160 kA with 1.7 MW of NBI-co to 240 kA with the addition of 1.7 MW of ICRH. More then 2/3 of the plasma current (340 kA) is then non-ohmically driven; the contribution of the bootstrap current to the latter amounts to 45 kA (Conrads et al., 1990). The changes of the target plasma parameters due to ICRH can only explain a 30 % increase of I_{tD}.

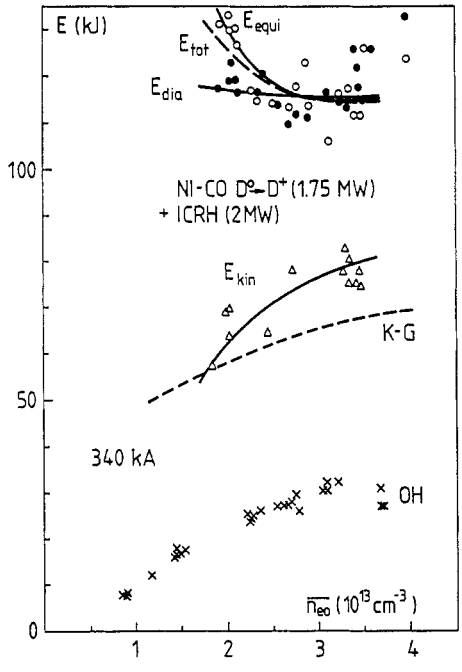

Fig. 9a Density scan of the energy for combined NBI-co + ICRH heating. The OH values and the K-G scaling predictions are also given.

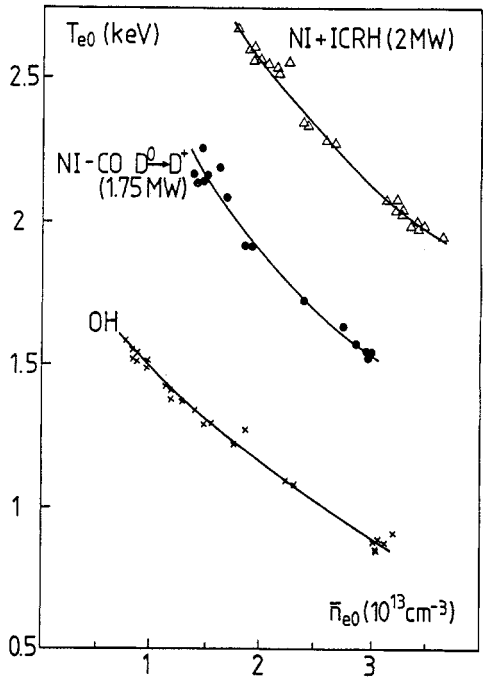

Fig. 9b Density scan of T_{eo} for OH, NBI-co and NBI-co + ICRH conditions.

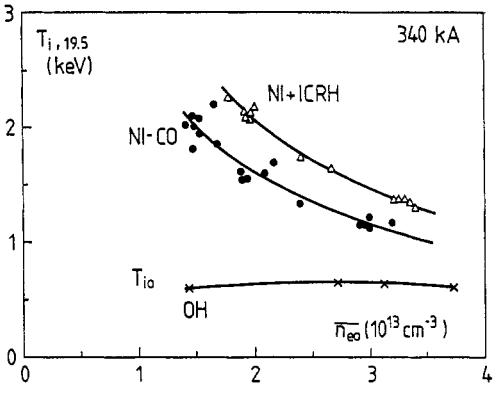

Fig. 9c Same as Fig. 9b but for T_{io}.

(iii) In combination with NBI-co, ICRH is capable of extending the density domain in which full stabilization of the sawtooth occurs or in which a given stretching of its period is present. This effect can be interpreted by the large increase of the perpendicular tail energy which leads to an enhanced trapped hot-ions population inside the q = 1 surface. In Fig. 8, it is seen that complete stabilization is not occuring with NBI-co at $\bar{n}_{eo} = 2 \times 10^{13}$ cm^{-3} but is occuring with the addition of ICRH. The rapid decrease of T_{eo} after the switch-off of both additional heating mechanisms is due to the crash of the monster sawtooth which occurs 10 ms later.

(iv) When the beam is present the neutron production is dominated by beam-plasma interaction. The application of ICRH with an equal amount of power as for NBI leads to an increase of the neutron yield

which may reach 80 %. This increase can be partly explained, as for the other effects, from the increase in the electron and ion temperature and possible changes in density of the target plasma but, in the best cases, a residual contribution remains unexplained. This is shown in Fig. 8 by the gap between the experimental curve Neu and the curve Neu,th which gives a theoretical prediction of the neutron yield. This prediction, which takes into account the beam and the target plasma characteristics, agrees well during the pure beam phase with the experiments but is unable to explain all the observed increases of the neutron yield during the combined heating (Van Wassenhove et al., 1990). This means that an additional interaction mechanism to that of the modification of the target plasma has to be invoked, for instance a direct acceleration of the beam ions by the RF fields, to explain the total neutron production as well as the total beam driven current.

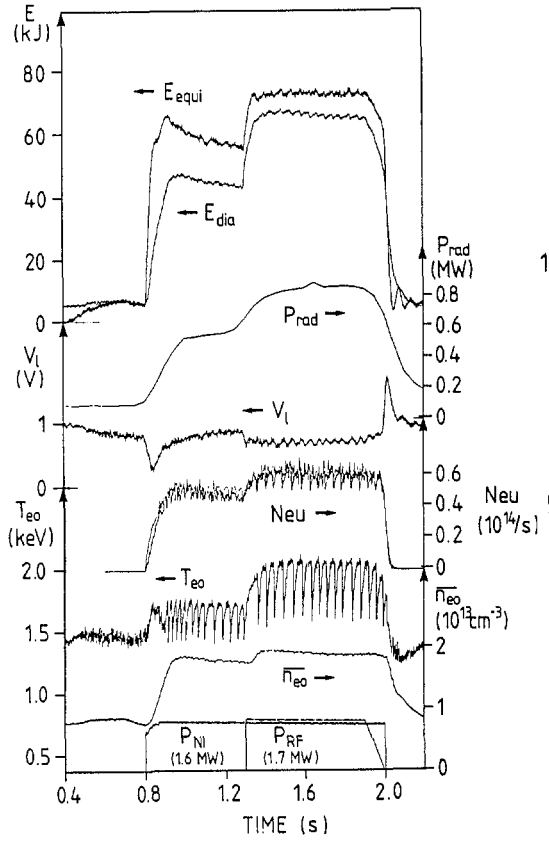

Fig. 10 Same as Fig. 8 but for NBI-counter and NBI-counter + ICRH (# 42092).

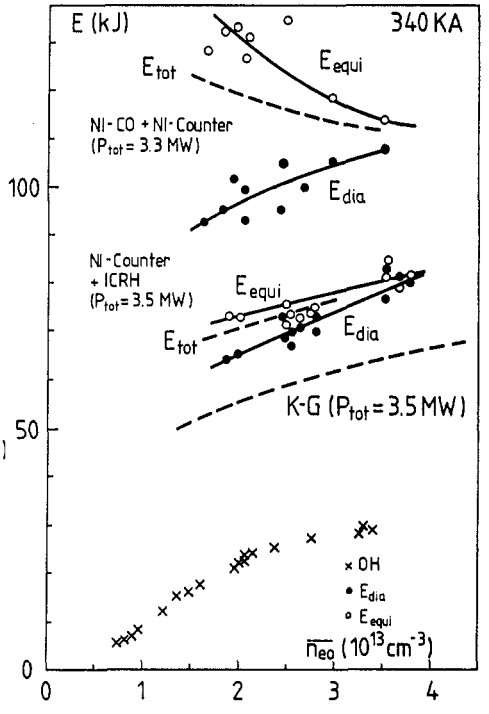

Fig. 11 Same as Fig. 9a but for NBI-counter + ICRH and NBI-counter + NBI-co.

5.2 Combined heating with counter-injection

(i) NBI-counter combined with ICRH.

Figure 10 shows the time evolution of a shot heated by counter-injection to which an equal amount of ICRH power is added. As for the combination NBI-co + ICRH, a more "isotropic" tail is produced by the addition of ICRH and P_{rad} does not increase in proportion to the increased P_{tot}; however for the same value of P_{tot} the energies and the central electron temperature are lower, and their increments with respect to the pure NBI heated conditions are also smaller. This appears also in the density scan of E_{dia}, E_{equi}, E_{tot} and T_{eo} given in figs. 11 and 12. Larger heating performances of NBI-co + ICRH with respect to NBI-counter + ICRH have also been observed in ASDEX (Ryter et al., 1989). A peaking of the density profile, comparable to those in the case of NBI-co + ICRH, also occurs. The loop voltage drop induced by ICRH is small. This can be interpreted as a partial cancellation of two opposite effects : the electron temperature and bootstrap current rise, leading to a V_ℓ drop and, as for

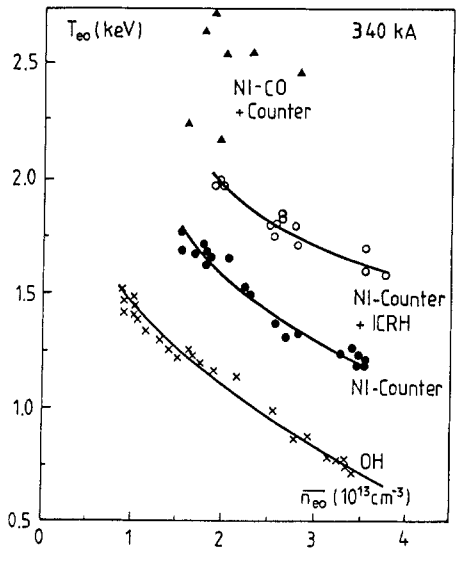

Fig. 12 T_{eo} versus $\bar{n}_{eo}$ for OH, NBI-counter, NBI-counter + ICRH and NBI-counter + NBI-co conditions. The conditions for combined heating are the same as in Fig. 11.

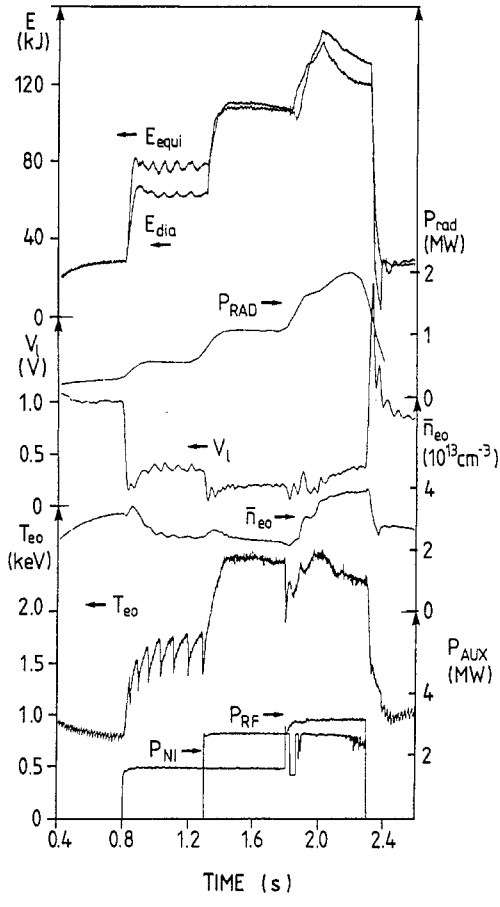

Fig.13 Same as Fig. 8 but for NBI-co followed by NBI-co + ICRH, followed by NBI-co + ICRH + NBI-counter heating with a total auxiliary power up to 5.9 MW (# 41122).

the combination NBI-co + ICRH, an increase of the beam driven current opposite to the plasma current. The effect of ICRH on the sawtooth stretching is much smaller than for its combination with NBI-co. Comparing Fig. 10 and Fig. 8, it is seen that the neutron yield (noted Neu) is smaller for NBI-counter heating but that it is also increased by the addition of ICRH.

(ii) NBI-counter combined with NBI-co.
A large scatter of the results is observed. It results from non stationary conditions due to a density rise during the heating pulse, sometimes accompanied by an impurity concentration increase. In Figs. 11 and 12 the best energy and T_{eo} results achieved up to now for balanced injection are shown. They are characterized by large energy anisotropy and a much higher value of E_{tot} than for the combination NBI-counter + ICRH for the same P_{tot}. The value of T_{eo} is also higher. The density profile becomes highly peaked, more than for the other combinations. The loop voltage roughly remains at the level reached with pure NBI-co. This indicates a compensation between the effect of the electron heating and of the bootstrap current increase and the drop in the total beam driven current. Complete sawtooth stabilization can also be achieved. A detailed study of its parametric dependence and its link with the theoretical explanation (Ongena et al., 1990) is still to be done.

(iii) All heating methods combined.
The addition of NBI-counter to a shot already heated by NBI-co + ICRH leads to the largest energy content and β_p (~1.5) reached in TEXTOR. An example is shown in Fig. 13. The characteristics are the same as for the combination NBI-counter + NBI-co, except that the energy tail becomes more

"isotropic" ($E_\perp \cong 2E_{//}$). Note the sawtooth stabilization which remains after an initial crash at the start of NBI-counter, the large $\bar{n}_{eo}$ rise which explains the lack of T_{eo} increase, the V_ℓ behaviour which remains initially to its level with NBI-co + ICRH. During the NBI-counter pulse an increase of the oxygen concentration is observed : this is to be correlated with the increase of P_{rad}, the decrease of E_{dia} and E_{equi} and the rise of V_ℓ which occur for t > 2 s.

(iv) Comparison between the combinations of two out of three methods.

In Table 2 a comparison is given between the best results of $\tau_{inc,tot}$, $\tau_{inc,kin}$ and η_e achieved for $\bar{n}_{eo}$ = 3 x 10^{13} cm^{-3} and I_p = 340 kA for the different combinations (with $P_{NI\text{-}co} \cong P_{NI\text{-}counter} \cong P_{RF}$). $\tau_{inc,kin}$ is not available for NBI-counter + ICRH due to the lack of T_i measurement.

Table 2 : τ_{inc} and η_e comparison ($\bar{n}_{eo}$ = 3 x 10^{13} cm^{-3}, I_p = 340 kA)

	unit	NBI-co + ICRH	NBI-count. + ICRH	NBI-count. + NBI-co
$\tau_{inc,tot}$	ms	24	14	28
$\tau_{inc,kin}$	ms	13	-	(21)
η_e	keV 10^{13} cm^{-3}/MW	1.0	0.75	1.5

For the combination NBI-co + NBI-counter, we use results of shot simulations by TRANSP yielding $E_{//} \sim 1.6\ E_\perp$ to evaluate E_{kin} from E_{dia} and E_{equi}. From Table 2, it results that the combinations NBI-co + ICRH and NBI-counter + NBI-co are roughly as effective for the total energy, T_{eo} increases and are more efficient than the combination NBI-counter + ICRH.

6. CONCLUSIONS

Different auxiliary heating methods and their combinations have been applied to and compared on TEXTOR. A large energy anisotropy is observed in all cases and has been studied in terms of the thermal and the tail part of the energy content. Large enhancement with respect to the Kaye-Goldston scaling is found as well with NBI-co or the combinations NBI-co + ICRH or NBI-co + NBI-counter even when the engineering value of P_{tot} is taken to compute the K-G scaling. For the total energy content E_{tot} the enhancement can reach about 2.3 for the latter two combinations at $\bar{n}_{eo}$= 1.75 x 10^{13} cm^{-3}. For the thermal energy E_{kin} the largest deviation is obtained for densities larger than 3 x 10^{13} cm^{-3} and reaches then 1.5 for the same heating combinations. With the three heating methods combined, a value of β_p = 1.5 has been reached corresponding to a β_t = 0.65 % which is equal to 70 % of the Troyon limit of 2.8 I_p (MA) / (a (m) x B_t (T)). It has been shown that complete sawtooth stabilization of the "monster" type can be obtained by the hot ion tail produced by NBI-co and that the density domain in which stabilization occurs can be significantly extended by the addition of ICRH (e.g. from n_{eo} < 1.5 x 10^{13} cm^{-3} up to n_{eo} < 2.25 x 10^{13} cm^{-3} by the addition of 1.4 MW of ICRH). Sawtooth stabilization is also observed for balanced injection. High non inductively driven current is observed with NBI-co which is increased by 50 % by the addition of ICRH, allowing to drive up to two third of the plasma current at low density ($\bar{n}_{eo}$ = 1.7 x 10^{13} cm^{-3}). The effect of counter beam driven current and of its increase in presence of ICRH is clearly seen with NBI - counter injection.

ACKNOWLEDGEMENTS

We thank R. Budny, R. Goldston and D. Mc Cune of PPPL for providing us with TRANSP and for their general support.

REFERENCES

Beuken, J.M. et al., (1988). Comparison of ICRH heating scenarii and antenna configurations in TEXTOR. Proc. 15th Eur. Conf. on Cont. Fusion and Plasma Heating, Dubrovnik, 1988, 12B, 174.

Conrads H. et al., (1989). Neutral beam heating of TEXTOR. Proc. 16th Eur. Conf. on Cont. Fusion and Plasma Physics, Venice, 1989, 13B, 1221.

Conrads H. et al., (1990). Proc. 13th Conf. on Plasma Physics and Contr. Nuclear Fusion Research, Washington, 1990.

Euringer H. et al., (1989). Neutral Injection for TEXTOR. Proc. IEEE 13 Symposium on Fusion Engineering, Knoxville, Vol II, 991.

Hawryluc R.J., (1980). *Physics of plasmas close to Thermonuclear Conditions*, edited by B. Coppi et al., Vol. 1, p. 19, ECE Brussels, 1980.

Kaye S.M., Goldston R.I., (1985). Global energy confinement scaling for neutral-beam-heated tokamaks. *Nuclear Fusion* , 25, 65.

Messiaen A.M. et al., (1989a). Effect of antenna phasing and wall conditioning on ICRH in TEXTOR. *Plasma Phys. contr. Fusion*, 31, 921.

Messiaen A.M. et al., (1989b). Preliminary results of combined ICRH-NBI heating in TEXTOR. Proc. 8th Topical Conference on Radio Frequency Power in Plasmas, Irvine, 1989, 362.

Ongena J. et al., (1990), this conference, 14B, 383.

Ryter F. et al., (1989). ICRF minority heating combined with counter neutral injection in ASDEX. Proc. 16th Eur. Conf. on Cont. Fusion and Plasma Physics, Venice, 1989, 13B, 1081.

Söldner et al., (1986). Study of profile control and supra-thermal electron production with lower hybrid waves. Report IPP III/111, Max Planck Institute for Plasma Physics, Garching; See also : Proc. 13 th Eur. Conf. on Contr. Fusion and Plasma Heating, Schliersee, 1986, 10C, part II, 319.

Van Wassenhove G. et al., (1990), this conference, 14B, 1040.

Weynants R.R. et al., (1989a). Heating and confinement studiae with low field side ICRH in TEXTOR. Proc. 12th Conf. on Plasma Physics and Controlled Nuclear Fusion Research, Nice, 1989, vol. 1, 571.

Weynants R.R. et al., (1989b). Analysis of ICRH induced minority particles and their effect on confinement and sawteeth. Proc. 16th Eur. Conf. on Cont. Fusion and Plasma Physics, Venice, 1989, 13B, 7.

Winter J. et al., (1989). Boronization in TEXTOR. *J. Nucl. Mater.* , 162-164 , 713.